

1       **Simulation of ozone-vegetation coupling and feedback in**  
2                   **China using multiple ozone damage schemes**

3  
4  
5                   Jiachen Cao<sup>1</sup>, Xu Yue<sup>1\*</sup>, Mingrui Ma<sup>2</sup>  
6

7   1. Jiangsu Key Laboratory of Atmospheric Environment Monitoring and Pollution  
8   Control, Collaborative Innovation Center of Atmospheric Environment and Equipment  
9   Technology, School of Environmental Science and Engineering, Nanjing University of  
10  Information Science & Technology (NUIST), Nanjing, 210044, China

11  2. State Key Laboratory of Pollution Control and Resource Reuse, School of the  
12  Environment, Nanjing University, Nanjing, 210044, China

13  
14  
15  
16  \*Corresponding author: Xu Yue

17  email: [yuexu@nuist.edu.cn](mailto:yuxu@nuist.edu.cn)  
18  
19  
20  
21  
22  
23  
24

## Abstract

As a phytotoxic pollutant, surface ozone ( $O_3$ ) not only affects plant physiology but also influences meteorological fields and air quality by altering leaf stomatal functions. Previous studies revealed strong feedbacks of  $O_3$ -vegetation coupling in China but with large uncertainties due to the applications of varied  $O_3$  damage schemes and chemistry-vegetation models. In this study, we quantify the  $O_3$  vegetation damage and the consequent feedbacks to surface meteorology and air quality in China by coupling two  $O_3$  damage schemes (S2007 vs. L2013) into a fully coupled regional meteorology-chemistry model. With different schemes and damaging sensitivities, surface  $O_3$  is predicted to decrease summertime gross primary productivity by 5.5%-21.4% and transpiration by 5.4%-23.2% in China, in which the L2013 scheme yields 2.5-4 times of losses relative to the S2007 scheme. The damages to photosynthesis of sunlit leaves are  $\sim 2.6$  times that of shaded leaves in the S2007 scheme but show limited differences in the L2013 scheme. Though with large discrepancies in offline responses, the two schemes yield similar magnitude of feedback to surface meteorology and  $O_3$  air quality. The  $O_3$ -induced damage to transpiration increases national sensible heat by 3.2-6.0 W  $m^{-2}$  (8.9% to 16.2%) while reduces latent heat by 3.3-6.4 W  $m^{-2}$  (-5.6% to -17.4%), leading to a 0.2-0.51  $^{\circ}C$  increase in surface air temperature and a 2.2-3.9% reduction in relative humidity. Meanwhile, surface  $O_3$  concentrations on average increase by 2.6-4.4  $\mu g m^{-3}$  due to the inhibitions of stomatal uptake and the anomalous enhancement in isoprene emissions, the latter of which is attributed to the surface warming by  $O_3$ -vegetation coupling. Our results highlight the importance of  $O_3$  control in China due to its adverse effects on ecosystem functions, global warming, and  $O_3$  pollution through the  $O_3$ -vegetation coupling.

**Keywords:** Ozone, vegetation, feedback, meteorology, air quality, regional model

## 52 **1 Introduction**

53 Surface ozone ( $O_3$ ) is one of the most enduring air pollutants affecting air quality  
54 in China, with detrimental effects on human health and ecosystem functions (Monk et  
55 al., 2015). Long-term observations and numerical simulations have shown that  $O_3$   
56 affects stomatal conductance (Li et al., 2017), accelerates vegetation aging (Feng et al.,  
57 2015), and reduces photosynthesis (Wittig et al., 2007). These negative effects altered  
58 carbon allocation (Yue and Unger, 2014; Lombardozzi et al., 2015) and inhibited plant  
59 growth (Li et al., 2016), suppressing ecosystem carbon uptake (Ainsworth, 2012).  
60 Moreover, these effects have profound implications for global/regional climate and  
61 atmospheric environment. Given the significant ecological impacts, a systematic  
62 quantification of the  $O_3$  vegetation damage effect in China is of great importance for  
63 the better understanding of the side effects of  $O_3$  pollution on both regional carbon  
64 uptake and climate change.

65 At present, field experiments on  $O_3$ -induced vegetation damage have been  
66 conducted in China but were mostly confined to individual monitoring sites. For  
67 instance, Su et al. (2017) conducted experiments on grassland in Inner Mongolia and  
68 found that elevated  $O_3$  concentrations resulted in a decrease of approximately 20% in  
69 the photosynthetic rate of herbaceous plants. Meta-analysis of tropical, subtropical, and  
70 temperate tree species in China found that increased  $O_3$  concentrations reduced net  
71 photosynthesis and total biomass of Chinese woody plants by 28% and 14%,  
72 respectively (Li et al., 2017). However, most of these experiments were conducted  
73 using open-top chambers with artificially controlled  $O_3$  concentrations, rather than  
74 actual surface  $O_3$  concentrations, making it difficult to quantitatively estimate the  
75 impact of ambient  $O_3$  on vegetation productivity. Furthermore, the spatial coverage of  
76 field experiments is limited, which hinders the direct use of observational data for  
77 assessing  $O_3$  vegetation damage in different regions of China.

78 Alternatively, numerical models provide a more feasible approach to quantify the  
79  $O_3$ -induced vegetation damage from the regional to global scales. Currently, there are  
80 three main parameterizations for the calculation of ozone vegetation damage. Felzer et

81 al. (2004) established an empirical scheme based on the Accumulated Ozone exposure  
82 over a Threshold of 40 ppb (AOT40) within the framework of a terrestrial ecosystem  
83 model. They further estimated that O<sub>3</sub> pollution in the United States led to a decrease  
84 in net primary productivity (NPP) by 2.6% to 6.8% during the period of 1980-1990.  
85 However, the AOT40 is related to O<sub>3</sub> concentrations alone and ignores the biological  
86 regulations on the O<sub>3</sub> stomatal uptake, leading to inconsistent tendencies between O<sub>3</sub>  
87 pollution level and plant damage at the drought conditions (Gong et al., 2021). In  
88 acknowledge of such deficit, Sitch et al. (2007) proposed a semi-mechanistic scheme  
89 calculating O<sub>3</sub> vegetation damage based on the stomatal uptake of O<sub>3</sub> fluxes and the  
90 coupling between stomatal conductance and leaf photosynthesis. Yue and Unger (2014)  
91 implemented this scheme into the Yale Interactive terrestrial Biosphere (YIBs) model.  
92 Taking into account varied O<sub>3</sub> sensitivities of different vegetation types, they estimated  
93 that surface O<sub>3</sub> led to reductions of 2-5% in the summer gross primary productivity  
94 (GPP) in eastern U.S. from 1998 to 2007. Later, Lombardozzi et al. (2013) conducted  
95 a meta-analysis using published chamber data and found different levels of responses  
96 to O<sub>3</sub> exposure between stomatal conductance and photosynthesis. They further  
97 implemented the independent response relationships into the Community Land Model  
98 (CLM) and estimated that current ozone levels led to a reduction in global GPP by 8%-  
99 12% (Lombardozzi et al., 2015).

100 The O<sub>3</sub> stress on vegetation physiology can feed back to affect regional climate.  
101 Lombardozzi et al. (2015) employed the CLM model and found that current O<sub>3</sub>  
102 exposure reduced transpiration by 2%-2.4% globally and up to 15% regionally over  
103 eastern U.S., Europe, and Southeast Asia, leading to further perturbations in surface  
104 energy balance. In U.S., Li et al. (2016) found that the O<sub>3</sub> vegetation damage reduced  
105 latent heat (LH) flux, precipitation, and runoff by 10-27 W m<sup>-2</sup>, 0.9-1.4 mm d<sup>-1</sup>, and  
106 0.1-0.17 mm d<sup>-1</sup>, respectively, and increased surface air temperature by 0.6-2.0 °C  
107 during the summer of 2007-2012. In China, Zhu et al. (2022) performed simulations  
108 and found that the inclusion of O<sub>3</sub>-vegetation interaction caused a 5-30 W m<sup>-2</sup> decrease  
109 in LH, 0.2-0.8 °C increase in surface air temperature, and 3% reduction in relative

110 humidity during summers of 2014-2017. Recently, Jin et al. (2023) applied a different  
111 regional model and estimated that O<sub>3</sub> exposure weakened plant transpiration and altered  
112 surface heat flux in China, resulting in significant increase of up to 0.16 °C in maximum  
113 daytime temperature and decrease of -0.74% in relative humidity. However, all these  
114 previous estimates of O<sub>3</sub>-induced feedback to climate were derived using the empirical  
115 O<sub>3</sub> damage scheme proposed by Lombardozzi et al. (2013), which assumed fixed  
116 damage ratios independent of O<sub>3</sub> dose for some vegetation species and as a result may  
117 have biases in the further estimated feedback to climate.

118 The O<sub>3</sub>-vegetation coupling also has intricate implications for air quality. On one  
119 hand, O<sub>3</sub>-vegetation coupling can influence meteorological conditions that affect O<sub>3</sub>  
120 generation, ultimately influencing the O<sub>3</sub> level (Sadiq et al., 2017). On the other hand,  
121 it can also influence biogenic emissions and dry deposition, thereby affecting O<sub>3</sub>  
122 concentrations (Gong et al., 2020). Sadiq et al. (2017) implemented O<sub>3</sub>-vegetation  
123 coupling in the Community Earth System Model (CESM) and estimated that surface  
124 O<sub>3</sub> concentrations increased 4-6 ppb in Europe, North America, and China due to O<sub>3</sub>-  
125 vegetation coupling. By using the CLM model with the empirical scheme of  
126 Lombardozzi et al. (2013), Zhou et al. (2018) found that O<sub>3</sub>-induced damage on leaf  
127 area index (LAI) could lead to changes in global O<sub>3</sub> concentrations by -1.8 to +3 ppb  
128 in boreal summer. Gong et al., (2020) used the O<sub>3</sub> damage scheme from Sitch et al.  
129 (2007) embedded in a global climate-chemistry-carbon coupled model and estimated  
130 that O<sub>3</sub>-induced stomatal inhibition led to an average surface O<sub>3</sub> increase of 1.2-2.1 ppb  
131 in eastern China and 1.0-1.3 ppb in western Europe. Different from the above global  
132 simulations with coarse resolutions, regional modeling with fine resolution can reveal  
133 more details about O<sub>3</sub>-vegetation coupling and feedback to surface O<sub>3</sub> concentrations  
134 in China (Zhu et al., 2022; Jin et al., 2023). However, all these regional simulations  
135 were carried out using O<sub>3</sub> damage scheme of Lombardozzi et al. (2013), limiting the  
136 exploration of model uncertainties due to varied O<sub>3</sub> vegetation damage schemes.

137 In this study, we implemented O<sub>3</sub> vegetation damage schemes from both Sitch et  
138 al. (2007) and Lombardozzi et al. (2013) into the widely-used regional meteorology-

139 chemistry model WRF-Chem. We validated the simulated meteorology and O<sub>3</sub>  
140 concentrations, and performed sensitivity experiments to explore the O<sub>3</sub> damage to GPP  
141 and consequent feedbacks to regional climate and air quality in China. Within the same  
142 framework, we compared the differences of O<sub>3</sub>-vegetation coupling from two schemes  
143 and explored the causes for the discrepancies. We aimed to quantify the modeling  
144 uncertainties in the up-to-date estimates of O<sub>3</sub> impact on regional carbon fluxes and its  
145 feedback to regional climate and air quality in China.

146

## 147 **2 Method**

### 148 **2.1 WRF-Chem model**

149 We used WRF-Chem model version 3.9.1 to simulate meteorological fields and  
150 O<sub>3</sub> concentration in China. The model includes atmospheric physics and dynamical  
151 processes, atmospheric chemistry, and biophysical and biochemical processes (Grell et  
152 al., 2005, Skamarock et al., 2008). The model domain is configured with 196 × 160 grid  
153 cells at 27 km horizontal resolution on the Lambert conformal projection, and covers  
154 the entire mainland China. In the vertical direction, 28 layers are set extending from  
155 surface to 50 hPa. The meteorological initial and boundary conditions were adopted  
156 from ERA5 reanalysis produced by the European Centre for Medium-Range Weather  
157 Forecasts (ECMWF) at a horizontal resolution of 0.25° × 0.25° (Hersbach et al., 2020).  
158 The chemical initial and boundary conditions were generated from the Model for Ozone  
159 and Related Chemical Tracer version 4 (MOZART-4), which is available at a horizontal  
160 resolution of 1.9° × 2.5° with 56 vertical layers (Emmons et al., 2010).

161 Anthropogenic emissions are adopted from the 0.25° Multi-resolution Emission  
162 Inventory for China (MEIC) and MIX Asian emission inventory for the other regions  
163 (available at <http://meicmodel.org>). Biogenic emissions are calculated online using the  
164 Model of Emissions of Gases and Aerosols from Nature (Guenther et al., 2006), which  
165 considers the impacts of plant types, weather conditions, and leaf area on vegetation  
166 emissions. Atmospheric chemistry is simulated using the Carbon Bond Mechanism  
167 version Z (CBMZ) (Zaveri and Peters, 1999) gas-phase chemistry module coupled with

168 a four-bin sectional Model for Simulating Aerosol Interactions and Chemistry  
 169 (MOSAIC) (Zaveri et al., 2008). The photolysis scheme is based on the Madronich  
 170 Fast-TUV photolysis module (Tie et al., 2003). The physical configurations include the  
 171 Morrison double-moment microphysics scheme (Morrison et al., 2009), the Grell-3  
 172 cumulus scheme (Grell et al., 2002), the Rapid Radiative Transfer Model longwave  
 173 radiation scheme (Mlawer et al., 1997), the Goddard short-wave radiation scheme  
 174 (Chou and Suarez, 1994), the Yonsei University planetary boundary layer scheme  
 175 (Hong et al., 2006), and the revised MM5 (Fifth generation Mesoscale Model) Monin–  
 176 Obukhov surface layer scheme.

177

## 178 **2.2 Noah-MP model**

179 Noah-MP is a land surface model coupled to WRF-Chem with multiple options  
 180 for key land-atmosphere interaction processes (Niu et al., 2011). Noah-MP considers  
 181 canopy structure with canopy height and crown radius, and depicts leaves with  
 182 prescribed dimensions, orientation, density, and radiometric properties. The model  
 183 employs a two-stream radiative transfer approach for surface energy and water transfer  
 184 processes (Dickinson, 1983). Noah-MP is capable of distinguishing photosynthesis  
 185 pathways between C<sub>3</sub> and C<sub>4</sub> plants, and defines vegetation-specific parameters for leaf  
 186 photosynthesis and respiration.

187 Noah-MP considers prognostic vegetation growth through the coupling between  
 188 photosynthesis and stomatal conductance (Farquhar et al., 1980; Ball et al., 1987). The  
 189 photosynthesis rate,  $A$  ( $\mu\text{molCO}_2 \text{ m}^{-2} \text{ s}^{-1}$ ), is calculated as one of three limiting factors  
 190 as follows:

$$191 \quad A_{tot} = \min(W_c, W_j, W_e)I_{gs} \quad (1)$$

192 where  $W_c$  is the RuBisco-limited photosynthesis rate,  $W_j$  is the light-limited  
 193 photosynthesis rate, and  $W_e$  is the export-limited photosynthesis rate.  $I_{gs}$  is the  
 194 growing season index with values ranging from 0 to 1. Stomatal conductance ( $g_s$ ) is  
 195 computed based on photosynthetic rate as follows:

$$196 \quad g_s = \frac{1}{r_s} = m \frac{A_{net}}{C_s} RH + b \quad (2)$$

197 where  $b$  is the minimum stomatal conductance;  $m$  is the Ball-Berry slope of the  
 198 conductance-photosynthesis relationship;  $A_{net}$  is the net photosynthesis by subtracting  
 199 dark respiration from  $A_{tot}$ ;  $C_s$  is the ambient CO<sub>2</sub> concentration at the leaf surface. The  
 200 assimilated carbon is allocated to various parts of vegetation (leaf, stem, wood, and root)  
 201 and soil carbon pools (fast and slow), which determines the variations of LAI and  
 202 canopy height. Plant transpiration rate is then estimated using the dynamic LAI and  
 203 stomatal conductance. Noah-MP also distinguishes the photosynthesis of sunlit and  
 204 shaded leaves. Sunlit leaves are more limited by CO<sub>2</sub> concentration while shaded leaves  
 205 are more constrained by insolation, leading to varied responses to O<sub>3</sub> damage.

206

### 207 **2.3 Scheme for ozone damage on vegetation**

208 We implemented the O<sub>3</sub> vegetation damage schemes proposed by Sitch et al. (2007)  
 209 (thereafter S2007) and Lombardozzi et al. (2013) (thereafter L2013) into the Noah-MP.  
 210 In S2007 scheme, the undamaged fraction  $F$  for net photosynthesis is dependent on the  
 211 sensitivity parameter  $a_{PFT}$  and excessive area-based stomatal O<sub>3</sub> flux, which is  
 212 calculated as the difference between  $f_{O_3}$  and threshold  $y_{PFT}$ :

$$213 \quad F = 1 - a_{PFT} \times \max\{f_{O_3} - y_{PFT}, 0\} \quad (3)$$

214 where  $a_{PFT}$  and  $y_{PFT}$  are specifically determined for individual plant functional types  
 215 (PFTs) based on measurements (Table 1). The stomatal O<sub>3</sub> flux  $f_{O_3}$  is calculated as

$$216 \quad f_{O_3} = \frac{[O_3]}{r_a + k_{O_3} \cdot r_s} \quad (4)$$

217 where  $[O_3]$  is the O<sub>3</sub> concentration at the reference level (nmol m<sup>-3</sup>),  $r_a$  is the  
 218 aerodynamic and boundary layer resistance between leaf surface and reference level (s  
 219 m<sup>-1</sup>).  $k_{O_3} = 1.67$  represents the ratio of leaf resistance for O<sub>3</sub> to that for water vapor.  $r_s$   
 220 represents stomatal resistance (s m<sup>-1</sup>). For S2007 scheme, stomatal conductance is  
 221 damaged with the same ratio (1- $F$ ) as photosynthesis and further affects O<sub>3</sub> uptake. In  
 222 Noah-MP, the  $f_{O_3}$  are calculated separately for sunlit and shaded leaves with  
 223 corresponding stomatal resistance (Supplementary Text S1).

224 As a comparison, the L2013 scheme applies separate O<sub>3</sub> damaging relationships



225 for photosynthetic rate and stomatal conductance. These independent relationships  
226 account for different plant groups and are calculated based on the cumulative uptake of  
227 O<sub>3</sub> (CUO) under different levels of chronic O<sub>3</sub> exposure. The leaf-level CUO (mmol m<sup>-2</sup>)  
228 <sup>2</sup>) is calculated by accumulating stomatal O<sub>3</sub> fluxes of Eq. (4) from the start of the  
229 growing season to the specific time step with mean LAI > 0.5 (Lombardozzi et al.,  
230 2012), when vegetation is most vulnerable to air pollution episodes. O<sub>3</sub> uptake is only  
231 accumulated when O<sub>3</sub> flux is above an instantaneous threshold of 0.8 nmol O<sub>3</sub> m<sup>-2</sup> s<sup>-1</sup>  
232 to account for ozone detoxification by vegetation at low O<sub>3</sub> levels (Lombardozzi et al.,  
233 2015). We also include a leaf-turnover rate for evergreen plants so that the accumulation  
234 of O<sub>3</sub> flux does not last beyond the average foliar lifetime. The O<sub>3</sub> damaging ratios  
235 depend on CUO with empirical linear relationships as follows:

$$236 F_{pO_3} = a_p \times CUO + b_p \quad (5)$$

$$237 F_{cO_3} = a_c \times CUO + b_c \quad (6)$$

238 where  $F_{pO_3}$  and  $F_{cO_3}$  are the ozone damage ratios for photosynthesis and stomatal  
239 conductance, respectively. The slopes ( $a_p$  for photosynthesis and  $a_c$  for stomatal  
240 conductance) and intercepts ( $b_p$  for photosynthesis and  $b_c$  for stomatal conductance) of  
241 regression functions are determined based on the meta-analysis of hundreds of  
242 measurements (Table 2). The ratios predicted in Eq. (5) and (6) are applied to  
243 photosynthesis and stomatal conductance, respectively, to account for their independent  
244 responses to O<sub>3</sub> damages. In Noah-MP, the  $F_{pO_3}$  and  $F_{cO_3}$  are calculated separately for  
245 sunlit and shaded leaves based on corresponding stomatal resistance (Supplementary  
246 Text S1).

247

## 248 **2.4 Observational data**

249 We validated the simulated meteorology and air pollutants with observations. The  
250 meteorological data were downloaded from the National Meteorological Information  
251 Center of China Meteorological Administration (CMA Meteorological Data Centre,  
252 2022, <http://data.cma.cn/data/detail/dataCode/A.0012.0001.html>). The daily averaged  
253 surface pressure (PRES), wind speed at a height of 10 m (WS10), relative humidity  
254 (RH) and temperature at a height of 2 m (T2) were collected from 839 ground stations.

255 Hourly surface O<sub>3</sub> concentrations at 1597 sites in China were collected from Chinese  
256 National Environmental Monitoring Center (CNEMC, <http://websearch.mep.gov.cn/>).

257

## 258 **2.5. Simulations**

259 We performed seven experiments to quantify the damaging effects of ambient O<sub>3</sub>  
260 on GPP and the feedbacks to regional climate and air quality (Table 3). All simulations  
261 are conducted from 1 May to 31 August of 2017 with the first month excluded from the  
262 analysis as the spin-up. The control simulations (CTRL) excluded the impact of ozone  
263 on vegetation. Three offline simulations were performed with the same settings as the  
264 CTRL run, except that O<sub>3</sub> vegetation damages were calculated and output without  
265 feedback to affect vegetation growth. These offline runs were established using either  
266 the S2007 scheme (Offline\_SH07 for high sensitivity and Offline\_SL07 for low  
267 sensitivity) or the L2013 scheme (Offline\_L13). As a comparison, three online  
268 simulations applied the S2007 scheme (Online\_SH07 for high sensitivity and  
269 Online\_SL07 for low sensitivity) and the L2013 scheme (Online\_L13) to estimate the  
270 O<sub>3</sub> damages to GPP, which further influenced LAI development, leaf transpiration, and  
271 dry deposition. The differences between CTRL and Online runs indicated the responses  
272 of surface meteorology and O<sub>3</sub> concentrations to the O<sub>3</sub>-induced vegetation damages.

273

## 274 **3. Results**

### 275 **3.1 Model evaluations**

276 We compared the simulated summer near-surface temperature, relative humidity,  
277 wind speed, and surface O<sub>3</sub> concentrations to observations. The model reasonably  
278 reproduces the spatial pattern of higher near-surface temperature in Southeast and  
279 Northwest and lower temperature over the Tibetan Plateau (Fig. 1a). On the national  
280 scale, the near-surface temperature is underestimated with a mean bias (MB) of 1.04 °C  
281 but it shows a high correlation (R=0.96). Unlike temperature, simulated relative  
282 humidity is overestimated with a MB of 5.04 % but a high R of 0.93 (Fig. 1b). Due to  
283 the modeling biases in the topographic effects, simulated wind speed is overestimated

284 by more than  $1.06 \text{ m s}^{-1}$  on the national scale (Fig. 1c). Such overestimation was also  
285 reported in other studies using WRF models (Hu et al., 2016, Liu et al., 2020, Zhu et  
286 al., 2022).

287 Comparisons with the measurements from air quality sites show that the simulated  
288  $\text{O}_3$  deviates from the observed mean concentrations by  $5.42 \mu\text{g m}^{-3}$  with a spatial R of  
289 0.68. The model reasonably captures the hotspots over North China Plain though with  
290 some overestimations, potentially attributed to uncertain emissions and coarse model  
291 resolutions. Such elevated bias in summer  $\text{O}_3$  is a common issue for both global and  
292 regional models over Asia. For example, Zhu et al. (2022) reported the overestimated  
293 summer average ozone concentration by  $13.82 \mu\text{g m}^{-3}$  in China. Liu et al. (2020)  
294 reached positive biases ranging from  $3.7 \mu\text{g m}^{-3}$  to  $13.32 \mu\text{g m}^{-3}$  using the WRF-CMAQ  
295 model. Overall, the WRF-Chem model shows reasonable performance in the simulation  
296 of surface meteorology and  $\text{O}_3$  concentrations in China.

297

### 298 **3.2 Offline $\text{O}_3$ damage**

299 We compared the offline  $\text{O}_3$  damage to photosynthesis between sunlit (PSNSUN)  
300 and shaded (PSNSHA) leaves during the summer. The S2007 scheme is dependent on  
301 instantaneous  $\text{O}_3$  uptake, which peaks in July when both  $\text{O}_3$  concentrations and stomatal  
302 conductance are high (Fig. S1 and S2). For the same  $\text{O}_3$  pollution level, the damages  
303 are much higher for the sunlit leaves (Fig. 2a-2b) than that for the shaded leaves (Fig.  
304 2d-2e), because of the higher stomatal conductance linked with the more active  
305 photosynthesis for the sunlit leaves. In contrast, the L2013 scheme depends on the  
306 accumulated  $\text{O}_3$  flux and assumes constant damages for some PFTs (Table 2), resulting  
307 in reductions of photosynthesis even at low  $\text{O}_3$  concentrations. The  $\text{O}_3$  damage to  
308 photosynthesis of sunlit and shaded leaves increases month by month, reaching a  
309 maximum in August (Fig. S1 and S2). We found limited differences in the  $\text{O}_3$  damages  
310 between sunlit (Fig. 2c) and shaded (Fig. 2f) leaves with L2013 scheme. Observations  
311 have reported that surface  $\text{O}_3$  has limited impacts on the shaded leaves (Wan et al.,  
312 2014), consistent with the results simulated by the S2007 scheme.

313 Figure 3 shows the effect of O<sub>3</sub> damage to stomatal resistance of sunlit (RSSUN)  
314 and shaded (RSSHA) leaves. Overall, the spatial pattern of the changes in stomatal  
315 resistance is consistent with those of photosynthesis (Fig. 2) but with opposite signs.  
316 Both RSSUN and RSSHA are enhanced by O<sub>3</sub> damage so as to prevent more O<sub>3</sub> uptake.  
317 For S2007 scheme, RSSUN with high and low sensitivities respectively increases by  
318 13.43% (Fig. 3a) and 8.35% (Fig. 3b), higher than the rates of 4.71% (Fig. 3d) and 2.97%  
319 (Fig. 3e) for RSSHA. These ratios are inversely connected to the changes of  
320 photosynthesis (Fig. 2), suggesting the full coupling of damages between leaf  
321 photosynthesis and stomatal conductance. For L2013 scheme, predicted changes in  
322 RSSUN (Fig. 3c) and RSSHA (Fig. 3f) are very similar with the magnitude of 25.3%-  
323 26.3%. These changes are higher than the loss of photosynthesis (Fig. 2c and 2f),  
324 suggesting the decoupling of O<sub>3</sub> damages to leaf photosynthesis and stomatal  
325 conductance as revealed by the L2013 scheme.

326 We further assessed the O<sub>3</sub> damage to GPP and transpiration (TR). For S2007  
327 scheme, O<sub>3</sub> causes damages to national average GPP and TR approximately by 5.5%  
328 with low sensitivity (Fig. 4b and 4e) and 8.4% with high sensitivity (Fig. 4a and 4d)  
329 compared to the CTRL simulation. The model predicts high GPP damages over North  
330 China Plain and moderate damages in the southeastern and northeastern regions. In the  
331 northwest, GPP damage is very limited due to the low relative humidity (Fig. 1b) that  
332 constrains the stomatal uptake. For L2013 scheme, TR shows uniform reductions  
333 exceeding -25% in most regions of China except for the northwest (Fig. 4f), though O<sub>3</sub>  
334 concentrations show distinct spatial gradient (Fig. 1d). The changes of GPP are similar  
335 to that of TR but with lower inhibitions (Fig. 4c). On average, the GPP reduction with  
336 the L2013 scheme is 2.5-3.9 times of that predicted with the S2007 scheme. The most  
337 significant differences are located in Tibetan Plateau with limited damages in S2007  
338 but strong inhibitions of both GPP and TR in L2013. The low temperature (Fig. 1a) and  
339 O<sub>3</sub> concentrations (Fig. 1d) jointly constrain O<sub>3</sub> stomatal uptake (Fig. S3), leading to  
340 low O<sub>3</sub> damages over Tibetan Plateau with the S2007 scheme. However, the L2013  
341 scheme applies  $b_p=0.8021$  for grassland (Table 2), suggesting strong baseline damages

342 up to 20% even with CUO=0 over Tibetan Plateau where the grassland dominates (Fig.  
343 S4).

344

### 345 **3.3 The O<sub>3</sub>-vegetation feedback to surface energy and meteorology**

346 The O<sub>3</sub> vegetation damage causes contrasting responses in surface sensible heat  
347 (SH) and LH (Fig. 5). For S2007 scheme, the SH fluxes on average increase by 3.17 W  
348 m<sup>-2</sup> (8.85%) with low sensitivity (Fig. 5b) and 5.99 W m<sup>-2</sup> (16.22%) with high  
349 sensitivity (Fig. 5a). The maximum enhancement is located in southern China, where  
350 the increased stomatal resistance (Fig. 3a) reduces transpiration and the consequent heat  
351 dissipation. Meanwhile, LH fluxes decrease by 3.26 W m<sup>-2</sup> (5.58%) with low sensitivity  
352 (Fig. 5e) and 6.43 W m<sup>-2</sup> (15.29%) with high sensitivity (Fig. 5d), following the  
353 reductions in transpiration (Fig. 4d and 4e). We found similar changes in surface energy  
354 by O<sub>3</sub>-vegetation coupling between the S2007 and L2013 schemes. The SH shows the  
355 same hotspots over southern China with national average increase of 12.85% (Fig. 5c),  
356 which is within the range of 8.85% to 16.22% predicted by the S2007 scheme. The LH  
357 largely decreases in central and northern China with the mean reduction of 17.4% (Fig.  
358 5f), close to the magnitude of 15.29% predicted with the S2007 scheme using the high  
359 O<sub>3</sub> sensitivity (Fig. 5d). Although the offline damages to GPP and TR are much larger  
360 with the L2013 than S2007 (Fig. 4), their feedback to surface energy shows consistent  
361 spatial pattern and magnitude (Fig. 5), likely because the O<sub>3</sub> inhibition in S2007 has the  
362 same diurnal cycle with energy fluxes while the L2013 scheme shows almost constant  
363 inhibitions throughout the day (Fig. S5). The zero or near-zero slope parameters ( $a_p$  and  
364  $a_c$ ) in the L2013 scheme (Table 2) lead to insensitive responses of photosynthesis and  
365 stomatal conductance to the variations of CUO. As a result, there were very limited  
366 diurnal variations in O<sub>3</sub> damage with the L2013 scheme. However, the strong nighttime  
367 damages in L2013 have limited contributions to the changes of surface energy, which  
368 usually peaks at the daytime.

369 The O<sub>3</sub>-induced damages to stomatal conductance weaken plant transpiration and  
370 thus slow down the heat dissipation at the surface, leading to the higher temperature but

371 lower RH in China (Fig. 6). On the national scale, temperature increases by 0.5 °C due  
372 to O<sub>3</sub> vegetation damage with the high sensitivity (Fig. 6a) and 0.23 °C with the low  
373 sensitivity (Fig. 6b) predicted using the S2007 scheme. A similar warming is predicted  
374 with the L2013 scheme except that temperature shows moderate enhancement over  
375 Tibetan Plateau (Fig. 6c). The average RH decreases by 3.68% with the high O<sub>3</sub>  
376 sensitivity (Fig. 6d) and 2.22% with the low sensitivity (Fig. 6e) in response to the  
377 suppressed plant transpiration. A stronger RH reduction of -3.85% is achieved with the  
378 L2013 scheme, which predicts the maximum RH reductions in the North (Fig. 6f).

379

### 380 **3.4 The O<sub>3</sub>-vegetation feedback to air quality**

381 The O<sub>3</sub>-induced inhibition on stomatal resistance leads to a significant increase in  
382 surface O<sub>3</sub> concentrations, particularly in eastern China (Fig. 7a-7c). The main cause of  
383 such feedback is the reduction in O<sub>3</sub> dry deposition, which exacerbates the O<sub>3</sub> pollution  
384 in China. For S2007 scheme, this positive feedback can reach up to 15 µg m<sup>-3</sup> with high  
385 sensitivity (Fig. 7a) and 8 µg m<sup>-3</sup> with low sensitivity (Fig. 7b) over North China Plain.  
386 On the national scale, surface O<sub>3</sub> enhances 4.40 µg m<sup>-3</sup> (5.08 %) with high O<sub>3</sub> sensitivity  
387 and 2.62 µg m<sup>-3</sup> (3.04%) with low O<sub>3</sub> sensitivity through the coupling to vegetation. For  
388 L2013 scheme, the changes of O<sub>3</sub> concentration (Fig. 7c) are comparable to that of the  
389 S2007 scheme with high sensitivity (Fig. 7a), except that the O<sub>3</sub> enhancement is  
390 stronger in the Southeast but weaker in the Northeast.

391 The O<sub>3</sub>-vegetation coupling also increases surface isoprene emissions. For S2007  
392 scheme, isoprene emissions increase by 6.13% with high sensitivity (Fig. 7d) and 3.43%  
393 with low sensitivity (Fig. 7e), with regional hotspots in North China Plain, northeastern  
394 and southern regions. The predictions using L2013 scheme (Fig. 7f) show very similar  
395 patterns and magnitude of isoprene changes to the S2007 scheme with high sensitivity.  
396 Such enhancement in isoprene emissions is related to the additional surface warming  
397 by O<sub>3</sub>-vegetation interactions (Fig. 6a-6c). In turn, the increased isoprene emissions  
398 contribute to the deterioration of O<sub>3</sub> pollution in China.

399

#### 400 **4. Conclusions and discussion**

401 In this study, we explored the feedback of O<sub>3</sub>-vegetation coupling to surface  
402 meteorology and air quality in China using two O<sub>3</sub> damage schemes embedded in a  
403 regional meteorology-chemistry coupled model. The two schemes predicted distinct  
404 spatial patterns with much larger magnitude of GPP loss in the L2013 scheme than that  
405 in the S2007 scheme. We further distinguished the leaf responses with different  
406 illuminations. For the S2007 scheme, the damages to photosynthesis of sunlit leaves  
407 are ~2.6 times of that to shaded leaves. However, for the L2013 scheme, limited  
408 differences are found between the sunlit and shaded leaves. The damages to leaf  
409 photosynthesis increase stomatal resistance, leading to the reductions of transpiration  
410 but enhancement of sensible heat due to the less efficient heat dissipation. These  
411 changes in surface energy and water fluxes feed back to increase surface temperature  
412 but decrease relative humidity. Although the L2013 scheme predicts much stronger  
413 offline damages, the feedback causes very similar pattern and magnitude in surface  
414 warming as the S2007 scheme. Consequently, surface O<sub>3</sub> increases due to the stomatal  
415 closure and isoprene emissions enhance due to the anomalous warming.

416 Our predicted O<sub>3</sub> damage to GPP was within the range of -4% to -40% as estimated  
417 in previous studies using different models and/or parameterizations over China (Ren et  
418 al., 2011; Lombardozzi et al., 2015; Yue et al., 2015; Sadiq et al., 2017; Xie et al., 2019;  
419 Zhu et al., 2022; Jin et al., 2023). Such a wide span revealed the large uncertainties in  
420 the estimate of O<sub>3</sub> impacts on ecosystem functions. In this study, we employed two  
421 schemes and compared their differences. With the S2007 scheme, we predicted GPP  
422 reductions of -5.5% to -8.5% in China. This is similar to the range of -4% to -10%  
423 estimated by Yue et al. (2015) using the same O<sub>3</sub> damage scheme. However, it is lower  
424 than the estimate of -12.1% predicted by Xie et al. (2019), likely due to the slight  
425 overestimation of surface O<sub>3</sub> in the latter study. With the L2013 scheme, we predicted  
426 much larger GPP reductions of -21.4%. However, such value was still lower than the -  
427 28.9% in Jin et al. (2023) and -20% to -40% in Zhu et al. (2022) using the same L2013  
428 scheme embedded in WRF-Chem model, though all studies showed similar spatial

429 patterns in the GPP reductions. Such differences were likely attributed to the varied  
430 model configuration as we ran the model from May while the other studies started from  
431 the beginning of years. The longer time for the accumulation of O<sub>3</sub> stomatal uptake in  
432 other studies might result in higher damages than our estimates with the L2013 scheme.

433 The O<sub>3</sub>-vegetation coupling caused strong feedback to surface meteorology and  
434 air quality. Our simulations with either scheme revealed that surface SH increases by  
435 2-28 W m<sup>-2</sup> and LH decreases by 4-32 W m<sup>-2</sup> over eastern China, consistent with the  
436 estimates of 5-30 W m<sup>-2</sup> by Zhu et al. (2022) using WRF-Chem model with the L2013  
437 scheme. Consequently, surface air temperature on average increases by 0.23-0.51°C  
438 while relative humidity decreases by 2.2-3.8%, similar to the warming of 0.2-0.8°C and  
439 RH reduction of 3% as predicted by Zhu et al. (2022). However, these changes in  
440 surface energy flux and meteorology are much higher than that in Jin et al. (2023),  
441 likely because the latter focuses on the perturbations averaged throughout the year  
442 instead of summer period as in this study and Zhu et al. (2022). We further predicted  
443 that O<sub>3</sub> vegetation damage increased surface O<sub>3</sub> by 1.0-3.33 μg m<sup>-3</sup> in China, similar  
444 to the 2.35-4.11 μg m<sup>-3</sup> estimated for eastern China using a global model (Gong et al.,  
445 2020). Regionally, the O<sub>3</sub> enhancement reached as high as 7.84-14.70 μg m<sup>-3</sup> in North  
446 China Plain, consistent with the maximum value of 11.76 μg m<sup>-3</sup> over the same domain  
447 predicted by Zhu et al. (2022). However, limited feedback to surface O<sub>3</sub> was predicted  
448 in Jin et al. (2023), mainly because the decreased dry deposition had comparable but  
449 opposite effects to the decreased isoprene emissions due to the reductions of LAI. Such  
450 discrepancy was likely caused by the stronger O<sub>3</sub> inhibition in Jin et al. (2023) following  
451 the longer period of O<sub>3</sub> accumulation, consequently exacerbating the negative impacts  
452 of LAI reductions on O<sub>3</sub> production.

453 There were some limitations in our parameterizations and simulations. First, we  
454 predicted increases of isoprene emissions in eastern China mainly due to the increased  
455 leaf temperature, which is in line with previous studies (Sadiq et al., 2017; Zhu et al.,  
456 2022). However, isoprene production is coupled to photosynthesis. There are empirical  
457 evidences showing that high dose of O<sub>3</sub> exposure reduces isoprene emissions when O<sub>3</sub>



458 exposure is prolonged enough to suppress photosynthesis (Bellucci et al., 2023).  
459 Inclusion of such negative feedback might alleviate the O<sub>3</sub>-induced enhancement in  
460 isoprene emissions. Second, the WRF-Chem model slightly overestimated summer O<sub>3</sub>  
461 concentrations, which could exacerbate the damages to stomatal conductance and the  
462 subsequent feedback. Third, the S2007 scheme employed the coupled responses in  
463 photosynthesis and stomatal conductance to O<sub>3</sub> vegetation damage. However, some  
464 observations revealed that stomatal response is slow under long-term O<sub>3</sub> exposure,  
465 resulting in loss of stomatal function and decoupling from photosynthesis (Calatayud  
466 et al., 2007; Lombardozzi et al., 2012). The L2013 scheme considered the decoupling  
467 between photosynthesis and stomatal conductance. However, this scheme shows no  
468 significant different changes for sunlit and shaded leaves. In addition, the calculation  
469 of CUO heavily relied on the O<sub>3</sub> threshold and accumulation period, leading to varied  
470 responses among different studies using the same scheme. Furthermore, the slopes of  
471 O<sub>3</sub> sensitivity in L2013 scheme were set to zero for some PFTs, leading to constant  
472 damages independent of CUO. Fourth, the current knowledge of the O<sub>3</sub> effects on  
473 stomatal conductance was primarily derived from leaf-level measurements (Matyssek  
474 et al., 2008), which were much fewer compared to that for photosynthesis. The limited  
475 data availability and lack of inter-PFT responses constrain the development of empirical  
476 parameterizations.

477 Despite these limitations, our study provided the first comparison of different  
478 parameterizations in simulating O<sub>3</sub>-vegetation interactions. We found similar feedbacks  
479 to surface energy and meteorology though the two schemes showed varied magnitude  
480 and distribution in the offline responses of GPP and stomatal conductance to surface  
481 O<sub>3</sub>. The main cause of such inconsistency lied in the low feedback of damages in L2013  
482 with some unrealistic inhibitions of ecosystem functions at night and over the regions  
483 with low O<sub>3</sub> level. Such similarity provides a solid foundation for the exploration of  
484 O<sub>3</sub>-vegetation coupling using different schemes. The positive feedback of O<sub>3</sub> vegetation  
485 damage to surface air temperature and O<sub>3</sub> concentrations posed emerging but ignored  
486 threats to both climate change and air quality in China.

487

488 **Data availability.** The observed hourly O<sub>3</sub> concentrations were obtained from Chinese  
489 National Environmental Monitoring Center (CNEMC, <http://websearch.mep.gov.cn/>).  
490 The observed meteorological data were obtained from the National Meteorological  
491 Information Center of China Meteorological Administration (CMA Meteorological  
492 Data Centre, 2022, <http://data.cma.cn/data/detail/dataCode/A.0012.0001.html>). The  
493 MEIC and MIX emission inventory are available at  
494 [http://meicmodel.org.cn/?page\\_id=560](http://meicmodel.org.cn/?page_id=560) and [http://meicmodel.org.cn/?page\\_id=89](http://meicmodel.org.cn/?page_id=89).

495

496 **Author contributions.** XY conceived the study. XY and JC designed the research and  
497 carried out the simulations. JC completed data analysis and the first draft. MM provided  
498 useful comments on the paper. XY reviewed and edited the manuscript.

499

500 **Competing interests.** The authors declare that they have no conflict of interest.

501

502 **Acknowledgements.** The authors are grateful to three anonymous reviewers for their  
503 constructive comments that have improved this study.

504

505 **Financial support.** This study was jointly funded by the National Key Research and  
506 Development Program of China (grant no. 2023YFF0805403), National Natural  
507 Science Foundation of China (grant no. 42293323), and Jiangsu Funding Program for  
508 Excellent Postdoctoral Talent (grant no. 2023ZB737).

509

## 510 **References**

511 Ainsworth, E. A., Yendrek, C. R., Sitch, S., Collins, W. J., and Emberson, L. D.: The  
512 effects of tropospheric ozone on net primary productivity and implications for  
513 climate change, *Annu. Rev. Plant Biol.*, 63, 637–661,  
514 <https://doi.org/10.1146/annurevarplant-042110-103829>, 2012.

515 Ball, J. T., Woodrow, I. E., and Berry, J. A.: A model predicting stomatal conductance  
516 and its contribution to the control of photosynthesis under different environmental

517 conditions, *Prog. Photosynthesis*, Springer, Dordrecht, 4, 221–224, 1987.

518 Bellucci, M., Locato, V., Sharkey, T. D., Gara D. and Loreto, F.: Isoprene emission by  
519 plants in polluted environments, *J PLANT INTERACT.*, 18:1, 2266463,  
520 <https://doi.org/10.1080/17429145.2023.2266463>, 2023

521 Calatayud, V., Cerveró, J., and Sanz, M. J.: Foliar, physiological and growth responses  
522 of four maple species exposed to ozone, *Water Air Soil Pollut.*, 185, 239–254,  
523 <https://doi.org/10.1007/s11270-007-9446-5>, 2007.

524 Chou, M. D. and Suarez, M. J.: An efficient thermal infrared radiation parameterization  
525 for use in general circulation models, *NASA Tech. Memo.*, 104506, 3, Maryland,  
526 USA, 85 pp., 1994.

527 Dickinson, R. E.: Land surface processes and climate – Surface albedos and energy  
528 balance, *Adv. Geophys.*, 25, 305–353, [https://doi.org/10.1016/S0065-](https://doi.org/10.1016/S0065-2687(08)60176-4)  
529 [2687\(08\)60176-4](https://doi.org/10.1016/S0065-2687(08)60176-4), 1983.

530 Emmons, L. K., Walters, S., Hess, P. G., Lamarque, J.-F., Pfister, G. G., Fillmore, D.,  
531 Granier, C., Guenther, A., Kinnison, D., Laepple, T., Orlando, J., Tie, X., Tyndall,  
532 G., Wiedinmyer, C., Baughcum, S. L., and Kloster, S.: Description and evaluation  
533 of the Model for Ozone and Related chemical Tracers, version 4 (MOZART-4),  
534 *Geosci. Model Dev.*, 3, 43–67, <https://doi.org/10.5194/gmd-3-43-2010>, 2010.

535 Farquhar, G. D., Caemmerer, S. V., and Berry, J. A.: A biochemical model of  
536 photosynthetic CO<sub>2</sub> assimilation in leaves of C<sub>3</sub> species, *Planta*, 149, 78–90,  
537 <https://doi.org/10.1007/bf00386231>, 1980.

538 Felzer, B., Kicklighter, D., Melillo, J., Wang, C., Zhuang, Q., and Prinn, R.: Effects of  
539 ozone on net primary production and carbon sequestration in the conterminous  
540 United States using a biogeochemistry model, *Tellus B*, 56, 230–248,  
541 <https://doi.org/10.1111/j.1600-0889.2004.00097.x>, 2004.

542 Feng, Z., Hu, E., Wang, X., Jiang, L., and Liu, X.: Ground-level O<sub>3</sub> pollution and its  
543 impacts on food crops in China: A review, *Environ. Pollut.*, 199, 42–48,  
544 <https://doi.org/10.1016/j.envpol.2015.01.016>, 2015.

545 Gong, C., Lei, Y., Ma, Y., Yue, X., and Liao, H.: Ozone–vegetation feedback through

546 dry deposition and isoprene emissions in a global chemistry–carbon–climate  
547 model, *Atmos. Chem. Phys.*, 20, 3841–3857, [https://doi.org/10.5194/acp-203841-](https://doi.org/10.5194/acp-203841-2020)  
548 2020, 2020.

549 Gong, C., Yue ,X., Liao, H., and Ma, Y.: A humidity-based exposure index representing  
550 ozone damage effects on vegetation, *Environ. Res. Lett.*, 16, 044030,  
551 <https://doi.org/10.1088/1748-9326/abecbb>, 2021.

552 Grell, G. A., McKeen, S., Michalakes, J., Bao, J.-W., Trainer, M., and Hsie, E.-Y.: Real-  
553 time simultaneous prediction of air pollution and weather during the Houston 2000  
554 Field Experiment, presented at the 4th Conference on Atmospheric Chemistry:  
555 Atmospheric Chemistry and Texas Field Study, 13–17 January, American  
556 Meteorological Society, Orlando, 2002.

557 Grell, G. A., Peckham, S. E., Schmitz, R., McKeen, S. A., Frost, G., Skamarock, W. C.,  
558 and Eder, B.: Fully coupled “online” chem- istry within the WRF model. *Atmos.*  
559 *Environ.*, 39, 6957–6975, <https://doi.org/10.1016/j.atmosenv.2005.04.027>, 2005.

560 Guenther, A., Karl, T., Harley, P., Wiedinmyer, C., Palmer, P. I., and Geron, C.:  
561 Estimates of global terrestrial isoprene emissions using MEGAN (Model of  
562 Emissions of Gases and Aerosols from Nature), *Atmos. Chem. Phys.*, 6, 3181–  
563 3210, <https://doi.org/10.5194/acp-6-3181-2006>, 2006.

564 Hersbach, H., Bell, B., Berrisford, P., Hirahara, S., Horányi, A., Muñoz-Sabater, J.,  
565 Nicolas, J., Peubey, C., Radu, R., Schepers, D., Simmons, A., Soci, C., Abdalla,  
566 S., Abellan, X., Balsamo, G., Bechtold, P., Biavati, G., Bidlot, J., Bonavita, M., De  
567 Chiara, G., Dahlgren, P., Dee, D., Diamantakis, M., Dragani, R., Flemming, J.,  
568 Forbes, R., Fuentes, M., Geer, A., Haimberger, L., Healy, S., Hogan, R. J., Hólm,  
569 E., Janisková, M., Keeley, S., Laloyaux, P., Lopez, P., Lupu, C., Radnoti, G., de  
570 Rosnay, P., Rozum, I., Vamborg, F., Villaume, S., and Thépaut, J.-N.: The ERA5  
571 global reanalysis, *Q. J. Roy. Meteor. Soc.*, 146, 1999–2049,  
572 <https://doi.org/10.1002/qj.3803>, 2020.

573 Hong, S.-Y., Noh, Y., and Dudhia, J.: A new vertical diffusion package with explicit  
574 treatment of entrainment processes, *Mon. Weather Rev.*, 134, 2318–2341,

575 <https://doi.org/10.1175/MWR3199.1>, 2006.

576 Hu, J., Chen, J., Ying, Q., and Zhang, H.: One-year simulation of ozone and particulate  
577 matter in China using WRF/CMAQ modeling system, *Atmos. Chem. Phys.*, 16,  
578 10333–10350, <https://doi.org/10.5194/acp-16-10333-2016>, 2016.

579 Jin, Z., Yan, D., Zhang, Z., Li, M., Wang, T., Huang, X., Xie, M., Li S and Zhuang.:  
580 Effects of elevated ozone exposure on regional meteorology and air quality in  
581 China through ozone-vegetation coupling. *J. Geophys. Res.-Atmos.*, 128,  
582 e2022JD038119. <https://doi.org/10.1029/2022JD038119>, 2023.

583 Li, J., Mahalov, A., and Hyde, P.: Simulating the impacts of chronic ozone exposure on  
584 plant conductance and photosynthesis, and on the regional hydroclimate using  
585 WRF/Chem, *Environ. Res. Lett.*, 11, 114017,  
586 <https://doi.org/10.1088/17489326/11/11/114017>, 2016.

587 Li, P., Calatayud, V., Gao, F., Uddling, J., and Feng, Z. Z.: Differences in ozone  
588 sensitivity among woody species are related to leaf morphology and antioxidant  
589 levels, *Tree Physiol.*, 36, 1105–1116, <https://doi.org/10.1093/treephys/tpw042>,  
590 2016.

591 Li, P., Feng, Z., Catalayud, V., Yuan, X., Xu, Y., and Paoletti, E.: A meta-analysis on  
592 growth, physiological, and biochemical responses of woody species to ground-  
593 level ozone highlights the role of plant functional types, *Plant Cell Environ.*, 40,  
594 2369–2380, <https://doi.org/10.1111/pce.13043>, 2017.

595 Liu, Y. and Wang, T.: Worsening urban ozone pollution in China from 2013 to 2017–  
596 Part 1: The complex and varying roles of meteorology, *Atmos. Chem. Phys.*, 20,  
597 6305–6321, <https://doi.org/10.5194/acp-20-6305-2020>, 2020.

598 Lombardozzi, D., Levis, S., Bonan, G., and Sparks, J. P.: Predicting photosynthesis and  
599 transpiration responses to ozone: decoupling modeled photosynthesis and stomatal  
600 conductance, *Biogeosciences*, 9, 3113–3130, <https://doi.org/10.5194/bg-9-31132012>, 2012.

602 Lombardozzi, D., Sparks, J. P., and Bonan, G.: Integrating O<sub>3</sub> influences on terrestrial  
603 processes: photosynthetic and stomatal response data available for regional and

604 global modeling, *Biogeosciences*, 10, 6815–6831, <https://doi:10.5194/bg-10->  
605 6815-2013, 2013.

606 Lombardozi, D., Levis, S., Bonan, G., Hess, P. G., and Sparks, J. P.: The influence of  
607 chronic ozone exposure on global carbon and water cycles, *J. Climate*, 28, 292–  
608 305, <https://doi.org/10.1175/JCLI-D-14-00223.1>, 2015.

609 Matyssek, R., Sandermann, H., Wieser, G., Booker, F., Cieslik, S., Musselman, R., and  
610 Ernst, D.: The challenge of making ozone risk assessment for forest trees more  
611 mechanistic, *Environ. Pollut.*, 156, 567–582,  
612 <https://doi:10.1016/j.envpol.2008.04.017>, 2008.

613 Mlawer, E. J., Taubman, S. J., Brown, P. D., Iacono, M. J., and Clough, S. A.: Radiative  
614 transfer for inhomogeneous atmosphere: RRTM, a validated correlated-k model  
615 for the longwave, *J. Geophys. Res-Atmos.*, 102(D14), 16663–16682,  
616 <https://doi.org/10.1029/97JD00237>, 1997.

617 Monks, P. S., Archibald, A. T., Colette, A., Cooper, O., Coyle, M., Derwent, R., Fowler,  
618 D., Granier, C., Law, K. S., Mills, G. E., Stevenson, D. S., Tarasova, O., Thouret,  
619 V., von Schneidmesser, E., Sommariva, R., Wild, O., and Williams, M. L.:  
620 Tropospheric ozone and its precursors from the urban to the global scale from air  
621 quality to short-lived climate forcer, *Atmos. Chem. Phys.*, 15, 8889–8973,  
622 <https://doi.org/10.5194/acp-15-8889-2015>, 2015.

623 Morrison, H., Thompson, G., and Tatarskii, V.: Impact of cloud microphysics on the  
624 development of trailing stratiform precipitation in a simulated squall line:  
625 comparison of one- and two-moment schemes, *Mon. Weather Rev.*, 137, 991–1007,  
626 <https://doi.org/10.1175/2008MWR2556.1>, 2009.

627 Niu, G. Y., Yang, Z. L., Mitchell, K. E., Chen, F., Ek, M. B., Barlage, M., Kumar, A.,  
628 Manning, K., Niyogi, D., Rosero, E., Tewari, M., and Xia, Y.: The community  
629 Noah land surface model with multiparameterization options (Noah-MP): 1.  
630 Model description and evaluation with local-scale measurements, *J. Geophys.*  
631 *Res-Atmos.*, 116, D12, <https://doi.org/10.1029/2010JD015139>, 2011.

632 Ren, W., Tian, H., Tao, B., Chappelka, A., Sun, G., Lu, C., Liu, M., Chen, G., and Xu,

633 X.: Impacts of tropospheric ozone and climate change on net primary productivity  
634 and net carbon exchange of China's forest ecosystems, *Glob. Ecol. Biogeogr.*, 20,  
635 391–406, <https://doi.org/10.1111/j.1466-8238.2010.00606.x>, 2011.

636 Sadiq, M., Tai, A. P. K., Lombardozzi, D., and Val Martin, M.: Effects of ozone–  
637 vegetation coupling on surface ozone air quality via biogeochemical and  
638 meteorological feedbacks, *Atmos. Chem. Phys.*, 17, 3055–3066,  
639 <https://doi.org/10.5194/acp-17-3055-2017>, 2017.

640 Sitch, S., Cox, P. M., Collins, W. J., and Huntingford, C.: Indirect radiative forcing of  
641 climate change through ozone effects on the land-carbon sink, *Nature*, 448, 791–  
642 794, <https://doi.org/10.1038/nature06059>, 2007.

643 Skamarock W C and Klemp J B. A time-split nonhydrostatic atmospheric model for  
644 weather research and forecasting applications. *J. Comput. Phys.*, 227(7): 3465–  
645 3485, <https://doi.org/10.1016/j.jcp.2007.01.037>, 2008.

646 Su, B., Zhou, M., Xu, H., Zhang, X., Li, Y., Su, H., and Xiang B.: Photosynthesis and  
647 biochemical responses to elevated O<sub>3</sub> in *Plantago major* and *Sonchus oleraceus*  
648 growing in a lowland habitat of northern China, *J. Environ. SCI.*, 53(3): 113–121,  
649 <https://doi.org/10.1016/j.jes.2016.05.011>, 2017.

650 Tie, X. X., Madronich, S., Walters, S., Zhang, R. Y., Rasch, P., and Collins, W.: Effect  
651 of clouds on photolysis and oxidants in the troposphere, *J. Geophys. Res.-Atmos.*,  
652 108, 4642, <https://doi.org/10.1029/2003jd003659>, 2003.

653 Wan, W., Manning, WJ., Wang, X., Zhang, H., Sun, X., and Zhang, Q.: Ozone and  
654 ozone injury on plants in and around Beijing, China, *Environ Pollut.*, 191: 215–  
655 222, <https://doi.org/10.1016/j.envpol.2014.02.035>, 2014

656 Wilkinson, S., Clephan, A. L., and Davies, W. J.: Rapid Low Temperature-Induced  
657 Stomatal Closure Occurs in Cold-Tolerant *Commelina Communis* Leaves But Not  
658 in Cold-Sensitive Tobacco Leaves, via a Mechanism That Involves Apoplastic  
659 Calcium But Not Abscisic Acid. *Plant Physiol.*, 126, 1566–1578.  
660 <https://doi.org/10.1104/pp.126.4.1566>, 2001.

661 Wittig, V. E., Ainsworth, E. A., and Long, S. P.: To what extent do current and projected

662 increases in surface ozone affect photosynthesis and stomatal conductance of trees?  
663 A metaanalytic review of the last 3 decades of experiments, *Plant Cell Environ.*,  
664 30, 1150–1162, <https://doi.org/10.1111/j.13653040.2007.01717.x>, 2007.

665 Xie, X., Wang, T., Yue, X., Li, S., Zhuang, B., Wang, M., and Yang, X.: Numerical  
666 modeling of ozone damage to plants and its effects on atmospheric CO<sub>2</sub> in China,  
667 *Atmos. Environ.*, 217, 116970, <https://doi.org/10.1016/j.atmosenv.2019.116970>,  
668 2019.

669 Yue, X. and Unger, N.: Ozone vegetation damage effects on gross primary productivity  
670 in the United States, *Atmos. Chem. Phys.*, 14, 9137–9153,  
671 <https://doi.org/10.5194/acp-14-9137-2014>, 2014.

672 Yue, X. and Unger, N.: The Yale Interactive terrestrial Biosphere model version 1.0:  
673 description, evaluation and implementation into NASA GISS ModelE2, *Geosci.*  
674 *Model Dev.*, 8, 2399–2417, <https://doi.org/10.5194/gmd-8-2399-2015>, 2015.

675 Zaveri, R. A., and Peters, L. K.: A new lumped structure photochemical mechanism for  
676 large-scale applications, *J Geophys Res-Atmos.*, 104, 30387-30415,  
677 <https://doi.org/10.1029/1999JD900876>, 1999.

678 Zaveri, R. A., Easter, R. C., Fast, J. D., and Peters, L. K.: Model for simulating aerosol  
679 interactions and chemistry (MOSAIC), *J. Geophys. Res-Atmos.*, 113, D13204,  
680 <https://doi.org/10.1029/2007JD008782>, 2008.

681 Zhou, S. S., Tai, A. P. K., Sun, S., Sadiq, M., Heald, C. L., and Geddes, J. A.: Coupling  
682 between surface ozone and leaf area index in a chemical transport model: strength  
683 of feedback and implications for ozone air quality and vegetation health, *Atmos.*  
684 *Chem. Phys.*, 18, 14133–14148, <https://doi.org/10.5194/acp-18-14133-2018>, 2018.

685 Zhu, J., Tai, A. P. K., and Yim, S. H. L.: Effects of ozone-vegetation interactions on  
686 meteorology and air quality in China using a two-way coupled land-atmosphere  
687 model, *Atmos. Chem. Phys.*, 22, 765-782, [https://doi.org/10.5194/acp-22-765-](https://doi.org/10.5194/acp-22-765-2022)  
688 2022, 2022.

689



690 **Tables**

691 **Table 1.** Parameters used for S2007 O<sub>3</sub> damage scheme <sup>a</sup>.

PFTs <sup>b</sup>	$a_{PFT}(\text{nmol}^{-1} \text{m}^2 \text{s})$ <sup>c</sup>	$\gamma_{PFT}(\text{nmol m}^{-2} \text{s}^{-1})$
EBF	0.075, 0.02	1.6
NF	0.075, 0.02	1.6
DBF	0.15, 0.04	1.6
SHR	0.1, 0.03	1.6
GRA	1.4, 0.25	5
CRO	1.4, 0.25	5

692 <sup>a</sup> The data source is Sitch et al. (2007).

693 <sup>b</sup> The plant functional types (PFTs) include evergreen broadleaf forest (EBF), needleleaf  
 694 forest (NF), deciduous broadleaf forest (DBF), shrubland (SHR), grassland (GRA), and  
 695 cropland (CRO).

696 <sup>c</sup> The first number is for high sensitivity and the second is for low sensitivity.

697

698

699

**Table 2.** Slopes and intercepts used for L2013 O<sub>3</sub> damage scheme <sup>a</sup>.

PFTs	$a_p$ (mmol m <sup>-2</sup> )	$b_p$	$a_c$ (mmol m <sup>-2</sup> )	$b_c$
EBF	0	0.8752	0	0.9125
NF	0	0.839	0.0048	0.7823
DBF	0	0.8752	0	0.9125
SHR	0	0.8752	0	0.9125
GRA	-0.0009	0.8021	0	0.7511
CRO	-0.0009	0.8021	0	0.7511

700

<sup>a</sup> The data source is Lombardozzi et al. (2015). Due to the data limit, we apply the same

701

sensitivity parameters for EBF, DBF, and SHR.

702

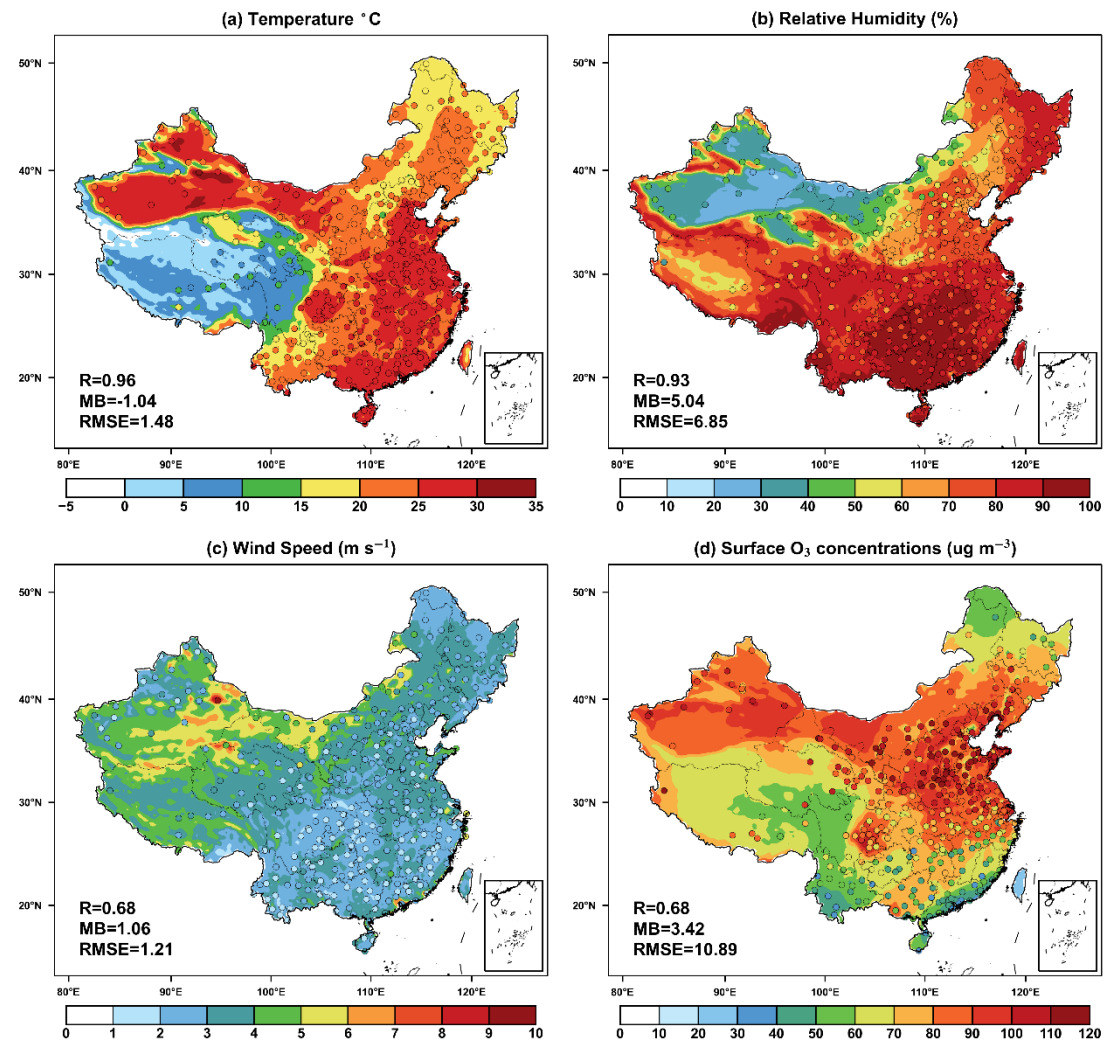
703

**Table 3.** Summary of simulation experiments

Name	O <sub>3</sub> damage to vegetable	Scheme
CRTL	-	-
Offline_SH07	High	Sitch et al. (2007)
Offline_SL07	Low	Sitch et al. (2007)
Offline_L13	-	Lombardozzi et al. (2013)
Online_SH07	High	Sitch et al. (2007)
Online_SL07	Low	Sitch et al. (2007)
Online_L13	-	Lombardozzi et al. (2013)

704

705



707

708

709

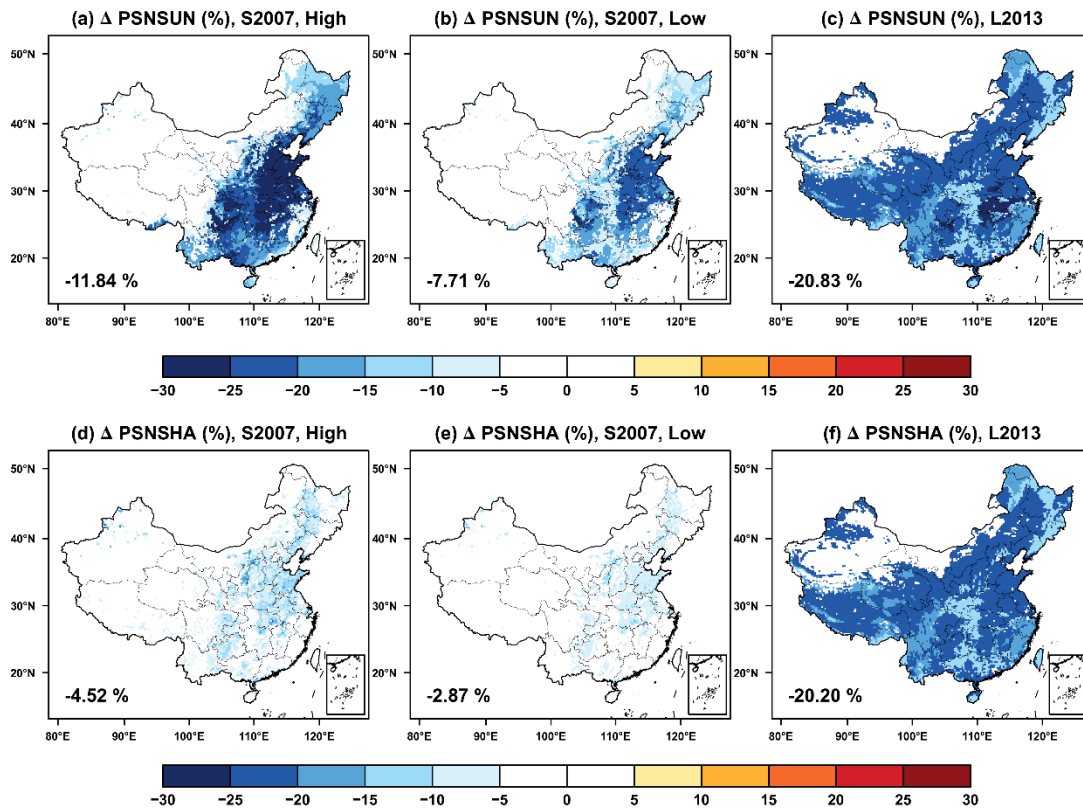
710 **Figure 1** Evaluations of simulated summer (June–August) daily (24-h average) (a)711 near-surface temperature, (b) relative humidity, (c) wind speed, and (d) surface  $\text{O}_3$ 

712 concentrations in China. The dots represent the site-level observations. The correlation

713 coefficients (R), mean biases (MB), and root-mean-square error (RMSE) for the

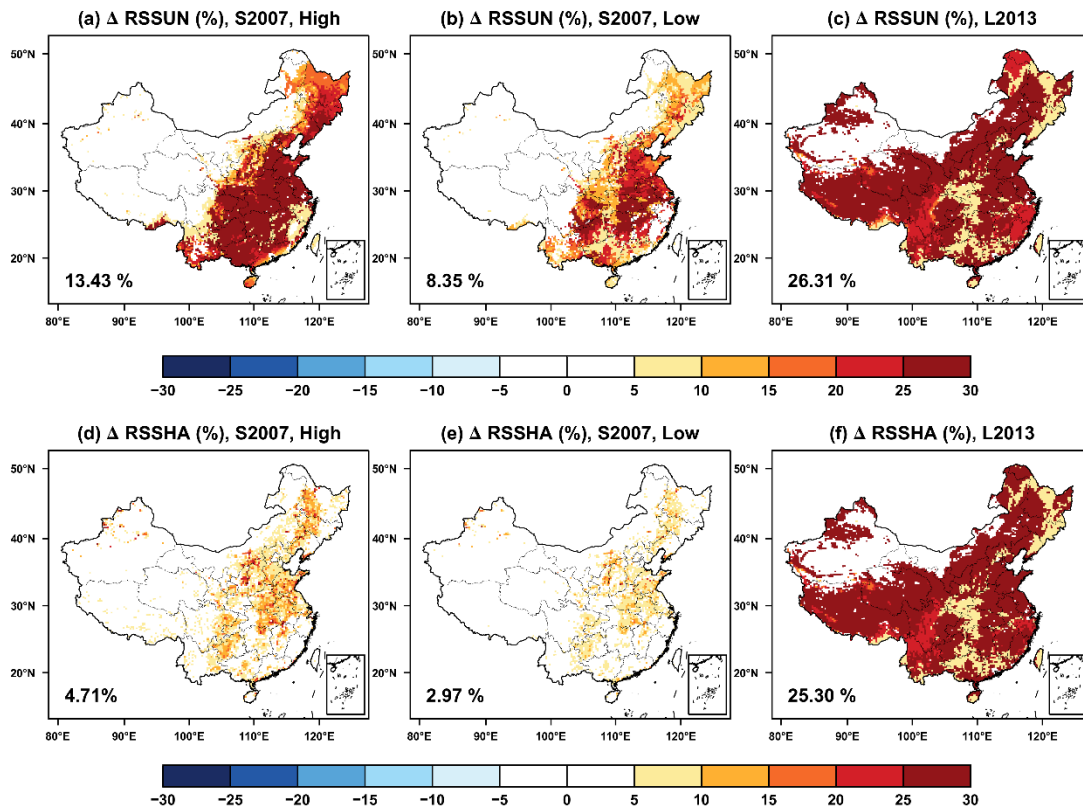
714 comparisons are shown in the lower left corner of each panel.

715



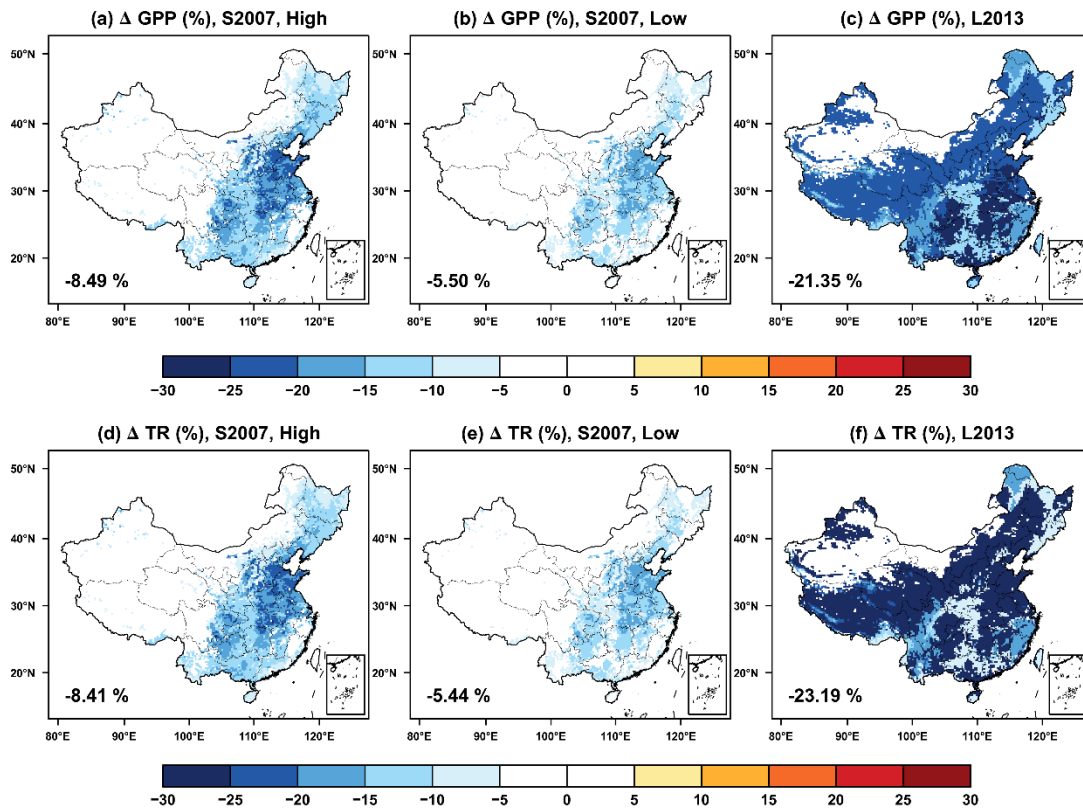
716  
 717  
 718  
 719  
 720  
 721  
 722

**Figure 2** Offline O<sub>3</sub> damage (%) to the summertime photosynthesis of (a-c) sunlit and (d-f) shaded leaves predicted by the S2007 scheme with (a, d) high and (b, e) low sensitivities or the (c, f) L2013 scheme. The area-weighted percentage changes are shown in the lower left corner.



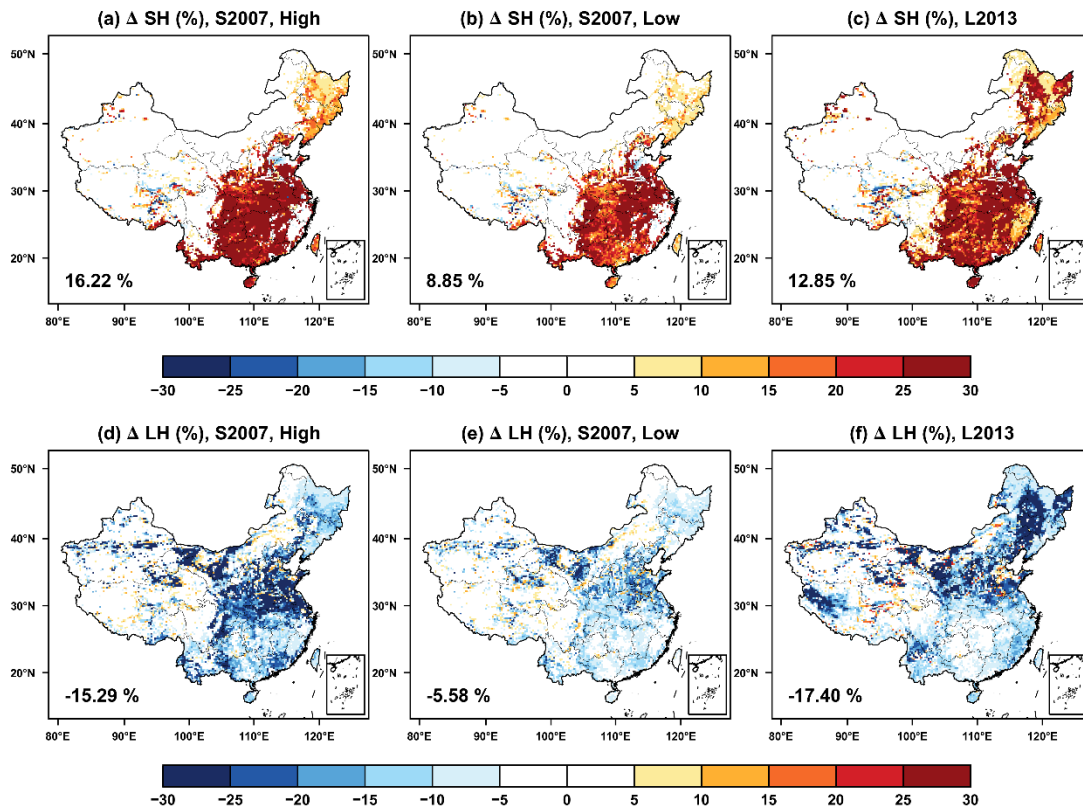
723  
 724  
 725  
 726

**Figure 3** The same as Fig. 2 but for the changes in stomatal resistance.



727  
 728  
 729  
 730  
 731  
 732  
 733

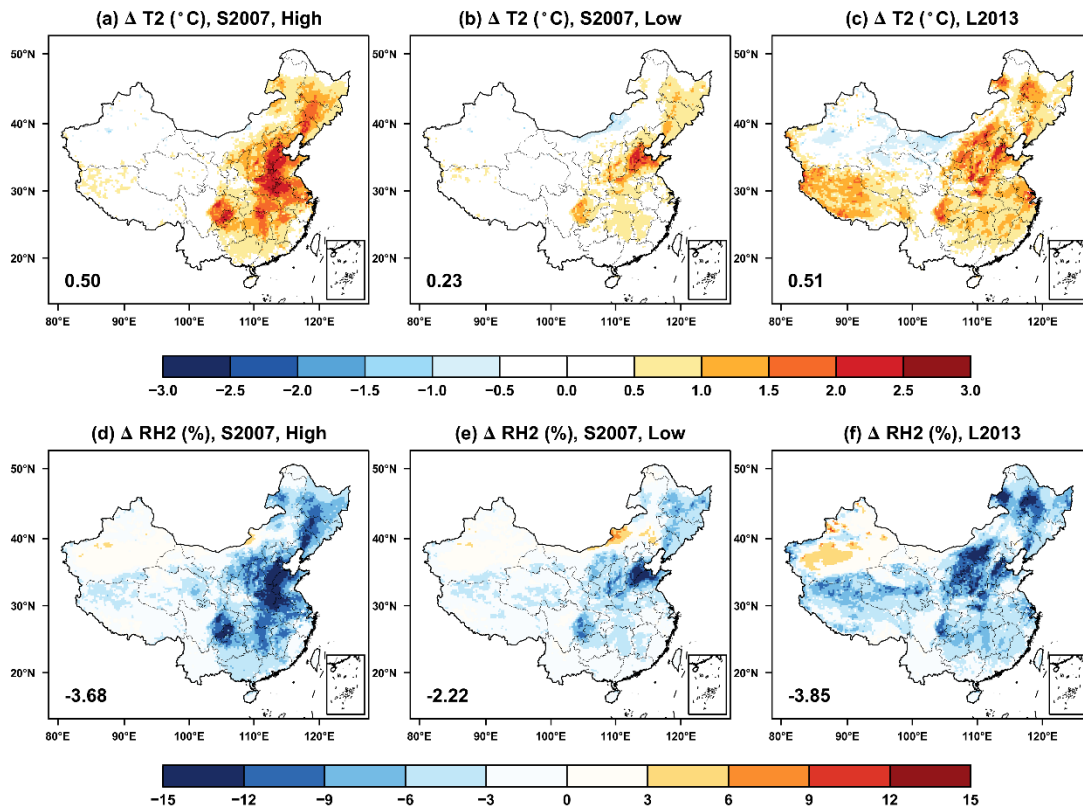
**Figure 4** Offline O<sub>3</sub> damage (%) to the (a-c) gross primary productivity (GPP) and (d-f) transpiration rate (TR) predicted by the Sitch scheme with (a, d) high and (b,e) low sensitivities or the (c, f) Lombardozzi scheme. The area-weighted percentage changes are shown in the lower left corner.



734  
735  
736  
737  
738  
739  
740  
741

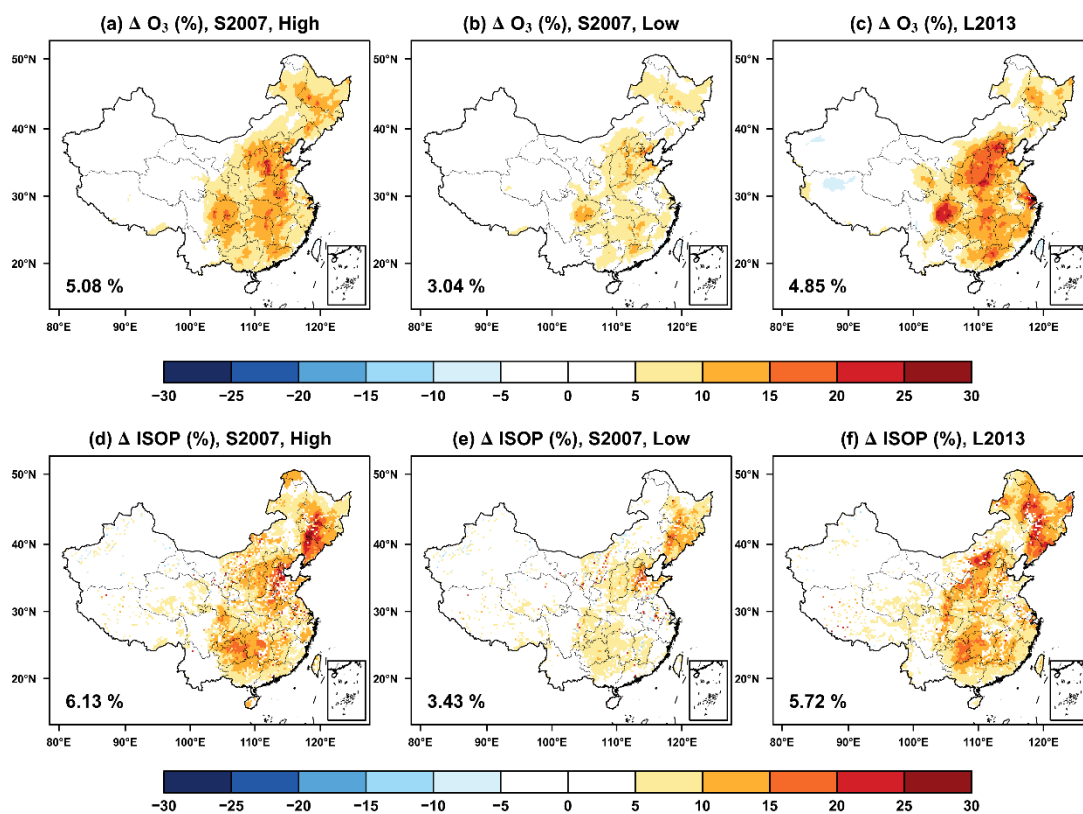
**Figure 5** The feedback of O<sub>3</sub>-vegetation interaction to surface (a-c) sensible and (d-f) latent heat fluxes in the summer predicted by the S2007 scheme with (a, d) high and (b, e) low sensitivities or the (c, f) L2013 scheme. The relative changes are shown with area-weighted percentage changes indicated at the lower left corner.





742  
 743  
 744  
 745  
 746  
 747

**Figure 6** The same as Fig. 5 but for changes in (top) air temperature and (bottom) relative humidity at 2 meters.



749

750

751 **Figure 7** The feedback of O<sub>3</sub>-vegetation interaction to surface O<sub>3</sub> concentrations and  
 752 isoprene emissions in the summer predicted by the S2007 scheme with (a, d) high and  
 753 (b, e) low sensitivities or the (c, f) L2013 scheme. The area-weighted percentage  
 754 changes are shown in the lower left corner.

755